Tip Clearance Effects on Inlet Hot Streaks Migration Characteristics in Low Pressure Stage of a Vaneless Counter-Rotating Turbine

Zhao Qingjun, Wang Huishe, Zhao Xiaolu and Xu Jianzhong
Institute of Engineering Thermophysics, Chinese Academy of Sciences
P.O. Box 2706, Beijing 100080, China
zhaoqingjun@mail.etp.ac.cn

Keywords: Vaneless Counter-Rotating Turbine, Hot streak, Secondary flow, Leakage flow

Abstract

In this paper, three-dimensional multiblade row unsteady Navier-Stokes simulations at a hot streak temperature ratio of 2.0 have been performed to reveal the effects of rotor tip clearance on the inlet hot streak migration characteristics in low pressure stage of a Vaneless Counter-Rotating Turbine. The hot streak is circular in shape with a diameter equal to 25% of the high pressure turbine stator span. The hot streak center is located at 50% of the span and the leading edge of the high pressure turbine stator. The tip clearance size studied in this paper is 2.0mm (2.59% high pressure turbine rotor height, and 2.09% low pressure turbine rotor height). The numerical results show that the hot streak is not mixed out by the time it reaches the exit of high pressure turbine rotor. The separation of colder and hotter fluid is observed at the inlet of low pressure turbine rotor. Most of hotter fluid migrates towards the rotor pressure surface, and only little hotter fluid migrates to the rotor suction surface when it convects into the low pressure turbine rotor. And the hotter fluid migrated to the tip region of the high pressure turbine rotor impinges on the leading edge of the low pressure turbine rotor after it goes through the high pressure turbine rotor. The migration of the hotter fluid directly results in very high heat load at the leading edge of the low pressure turbine rotor. The migration characteristics of the hot streak in the low pressure turbine rotor are dominated by the combined effects of secondary flow and leakage flow at the tip clearance. The leakage flow trends to drive the hotter fluid towards the blade tip on the pressure surface and to the hub on the suction surface, even partial hotter fluid near the pressure surface is also driven to the rotor suction surface through the tip clearance. Compared with the case without rotor tip clearance, the heat load of the low pressure turbine rotor is intensified due to the effects of the leakage flow. And the numerical results also indicate that the leakage flow effect trends to increase the low pressure turbine rotor outlet temperature at the tip region.

Introduction

A Vaneless Counter-Rotating Turbine (VCRT) is composed of a highly loaded single stage high pressure turbine (HPT) and a single stage vaneless counter-rotating low pressure turbine/rotor (LPT/LPR). Due to the parts elimination and size reduction, the VCRT can offer some significant benefits compared with conventional two stage turbine, even 1+1 counter-rotating turbine, such as the elevated thrust-to-weight ratio of aero-engine, the improved performance of aircraft, the reduced cooling flow, and so on (Keith et al., 2000, [1]; Haldeman et al., 2000, [2]; Zhao, et al., 2006, [3, 4]). From the 1950s, counter-rotating turbines have been carefully investigated (Wintucky, et al., 1958, [5]; Louis, 1985, [6]; Zhao, et al., 2006, [3, 4]). GE has also been developing Counter-Rotating Turbine Systems (CRTS) since the 1980s. And the CRTS will apply to GEnx engines in the future. It indicates that the CRTS will also be selected in airline engines for the aim of economy.

Experimental data taken from gas turbine combustors indicate that the flow exiting the combustor can contain both circumferential and radial temperature gradients. The phenomenon is known as hot streaks. The hot streaks arise from the combination of the combustor core flow with the combustor bypass and combustor surface cooling flows. In turbine, the hot streaks convect through the vanes and interact with the rotor blades. They can cause local hot spots on the blade surfaces, leading to heat fatigue of blade and reducing blade life.

An earlier research on streamline pattern showed theoretically that inflow temperature gradients will not alter the streamline pattern in vanes as long as the inflow total pressure is uniform (Munk and Prim, 1947, [7]). However, the following research on the secondary flow of rotating system, which was performed by Lakshminarayana and Horlock (1973, [8]), indicated that inflow temperature nonuniformities can lead to secondary flow in the rotating blade rows. Butler et al. (1989, [9]) carried out an experimental investigation on hot streak migration using the Large-Scale Rotating Rig (LSRR), which is often used in hot streaks investigations. They also found the temperature gradients have not altered the flow within the turbine stator but to have significant impact on the flowfield of rotor blade rows when the total pressure in the distortion is uniform. Their conclusion had been verified by some other experimental and numerical investigations (Rai and Dring, 1990, [10]; Roback and Dring, 1992, [11]; Dorney et al. 1992, [12]; Dorney and Davis, 1993, [13], Dorney, 1996, [14]). The results, which were obtained by Butler et al. (1989, [9]), Sharma et al. (1990, [15]) , Roback and Dring (1992, [11]) by experimental and numerical investigations, showed that hot streaks cause hotter gas to accumulate on the rotor blade pressure surfaces

and colder gas to accumulate on the rotor blade suction surfaces. However, the numerical investigation results of Gundy-Burlet and Dorney (1996, [16]) indicated that the migration patterns of hot streaks are directly related to the position of the hot streak in relation to the first-stage stator. When the hot streak impinges the leading edge (LE) of the first-stage stator, the hot gases are convected with the stator wake and migrate to the suction surface (SS) of the first-stage rotor. On the contrary, the hot gases migrate to the pressure surface (PS) of the first-stage rotor when the hot streak is located in the midpitch of the first-stage stator vanes. The different characteristic of hot streaks migration in rotor blade rows should be investigated in detail. In addition to secondary flow and circumferentially relative location effect, Shang and Epstein (1997, [17]) showed that hot streak migration is also affected by buoyancy, which tends to drive the hot streak toward the hub.

The experimental facilities most often used in hot streak investigations include the Large-Scale Rotating Rig (LSRR) (Butler et al. 1989, [9]; Roback and Dring, 1992, [11]; Dring et al. 1987, [18] ; Sharma et al. 1997, [19]), NASA Warm Core Turbine Test Rig (WCTTR) (Whitney et al. 1980, [20]; Schwab et al. 1983, [21]; Stabe et al. 1984, [22]) and MIT Blowdown Turbine Test Rig (BTTR) (Guenette, 1985, [23]; Sujudi, 1994, [24]; Shang. 1995, [25]). The LSRR experiments were performed at low speed, but blade surface temperature (CO2 concentrations) was measured. In the WCTTR experiments, blade surface temperature was not measured, but it is a high speed rig. Comparing with LSRR and WCTTR, BTTR experiments not only were performed at high speed, but also blade surface temperature can been measured. Shang et al. (1995, [26]) performed hot streak experiments using BTTR in MIT in order to examine the effects of hot streak migration on blade surface temperature at high speed.

Harasgama (1990, [27]) performed a numerical simulation of radial temperature distortion at inlet to a rotating turbine rotor. The results show that the hot gas is transported to the pressure surface of the blade and that hot gas also migrates to the blade pressure side tip. At locations greater than 50-60% axial chord the hot gas enters the tip-gap and emerges over the suction side. The results also indicate that the secondary flows within the turbine rotor are enhanced by the introduction of inlet radial temperature distortion. The heat flux near the tip region on the pressure side of the blade can be increased by up to 76% due to the redistribution of the inlet temperature distortion. The numerical investigations preformed by Gundy Burlet (1997, [28]) show that the hot streak directly impinged on the leading edge of the first-stage stator results in low levels of heat transfer on the second-stage stator. And the results illustrate that relatively high heat transfer on the first-stage rotor is localized to the leading edge, hub vortex and tip leakage flow regions. Castillon et al. (2003, [29]) carried out an unsteady 3-D numerical analysis on a hot streak transport through an axial high pressure turbine stage. The predicted results confirm the conclusion: if the hot streak is located in front of the NGV leading edge, the rotor blade experiences significant heat transfer reduction compared to an inlet mid-passage location. And the reattachment lines rooted in the tip leakage vortex were observed around 90% span of the rotor. The results also show that the hot gas driven on the pressure surface of the rotor can convect into the tip-gap and migrate to the suction surface.

In this paper, the effects of tip clearance on the inlet hot streaks migration characteristics in the low pressure stage of the VCRT will be explored by means of 3-D unsteady numerical simulations.

Numerical algorithm

NUMECA software systems are employed to study this problem. The numerical method is described in details in the user manual (2005, [30]). Here only a brief description about the main features is reported.

The governing equations in NUMECA are the time dependent, three-dimensional Reynolds-averaged Navier-Stokes equations. The solver of NUMECA is FINE/Turbo and it is based on a cell centered finite volume approach, associated with a central space discretization scheme together with an explicit four-stage Runge-Kutta time integration method.

Residual smoothing, local time-stepping, and multi-gridding are employed to speed up convergence to the steady state solution. The dual time stepping method (Jameson, 1991, [31]; Arnone and Pacciani, 1996, [32]) and Domain Scaling method (Rai, 1989, [33]) are used to perform time accurate calculations.

Various turbulence models have been included in the solver for the closure of governing equations. The widely used approach based on one transport equation (Spalart and Allmaras, 1992, [34]) has been selected in this paper. The Spalart-Allmaras model has become quite popular in the last years because of its robustness and its ability to treat complex flows. The main advantage of Spalart-Allmaras model when compared to the one of Baldwin-Lomax is that the turbulent eddy viscosity field is always continuous. Its advantage over the k-ε model is mainly its robustness and the lower additional CPU and Memory usage.

The time step limitations arising from the turbulent source terms are accounted for in the model so that computations can be performed with the maximum allowable CFL number without penalizing numerical efficiency.

Boundary conditions

The theory of characteristics is used to determine the boundary conditions at the inlet and exit of computational domain. At the inlet, total pressure, total temperature and circumferential and radial flow angles are specified as many constants in the simulation without inlet hot streak. While in those simulations with inlet hot streaks, the inlet total temperature is specified as a function of the spatial coordinates. And the total pressure and the circumferential and radial

flow angles are still given as many constants at the inlet. Due to selecting the Spalart-Allmaras turbulence model, the kinematic turbulent viscosity should be specified in the inlet boundary conditions. In this paper, it is $0.0001 m^2/s$.

In these simulations with inlet hot streaks, the flow variables in the hot streak must be modified. In the hot streak, the inlet flow variables used to define the specified boundary conditions can be written as:

$$\begin{aligned} u_{hs} &= u_\infty \sqrt{T_{hs}/T_\infty} \qquad v_{hs} = v_\infty \sqrt{T_{hs}/T_\infty} \\ w_{hs} &= w_\infty \sqrt{T_{hs}/T_\infty} \qquad P_{hs} = P_\infty \\ a_{hs} &= a_\infty \sqrt{T_{hs}/T_\infty} \qquad \rho_{hs} = \rho_\infty / (T_{hs}/T_\infty) \end{aligned} \tag{1}$$

where T_{hs} is the static temperature within the hot streak and T_∞ is the static temperature of the unaffected inlet flow. The static pressure and total pressure within the hot streak are assumed to be equal to that of the unaffected inlet flow.

At the exit, the circumferential and radial velocity components, entropy and the downstream running Riemann invariant are extrapolated from the interior of the computational domain. The static pressure, P_6 ,is specified at the hub of the exit and the static pressure values at all other radial locations are obtained by integrating the equation for radial equilibrium. Periodicity is enforced along the outer boundaries of H-O-H grids in the circumferential direction.

No-slip boundary conditions should be enforced at solid wall surfaces for viscous simulations. In this paper, absolute no-slip boundary conditions are enforced at the hub and tip end walls of the HPT stator regions, along the surface of the HPT vane, and along the casing walls of the HPT rotor and LPR regions. Relative no-slip boundary conditions are imposed at the hub end walls of the HPT rotor and LPR regions, and the surfaces of the HPT rotor and LPR blades. It is assumed that the normal derivative of pressure is zero at the solid wall surfaces, and that the walls are adiabatic.

Vaneless Counter-Rotating Turbine

The VCRT studied in this paper is composed of a highly loaded single stage HPT coupled with a vaneless counter-rotating LPT/LPR. It has high expansion ratio and operates in transonic regimes. The VCRT has some unique characteristics, which are different from the conventional two stage turbine, even 1+1 counter-rotating turbine. These characteristics include:

- The HPT rotor and LPT/LPR are counter-rotating.
- The LPT is vaneless.
- There are high relative Mach number (~1.5) and relative flow angle (~70°) at the outlet of the HPT.

The design conditions of the VCRT are shown in Table 1.

Table 1: The flow conditions in the VCRT

Inlet total temperature (K)	500
Inlet total pressure (kPa)	300
Mass flow (kg/s)	17.7
Rotational speed of HPT rotor (RPM)	6970
Rotational speed of LPR (RPM)	-6970
Expansion ratio of HPT	2.93
Expansion ratio of LPT	2.07
SWR	1.77

The airfoil counts in the steady and unsteady model are reduced from the actual count 36/36/36 for the HPT stator, HPT rotor and LPR, respectively, to 1/1/1 for computational efficiency. The tip clearance size studied in this paper is 2.0mm (2.59% HPT rotor height and 2.09% LPR height) (see Fig.1). The typical y^+ values of less than 15 are used at the boundaries. All of these results in CFD models with about 0.42 (without tip-gap) and 0.57 (with tip-gap) million grid points employing a sheared "H-O-H" mesh generated by NUMECA AutoGrid (see Table 2 and Fig. 2). It will take about one week to compute an unsteady case using a 3.0GHz one-Intel-CPU computer. According to the past experiences, which were obtained in the steady three-dimensional viscous analyses about the VCRT (Zhao et al., 2006, [4]), the grid size in the Table 2 is adequate to the investigation in this paper.

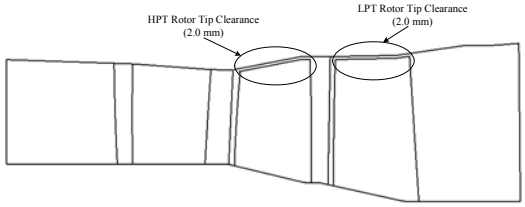

Fig. 1: Meridional section of the VCRT with rotor tip-gap

Table 2: Grid dimensions (*i*-azimuthal direction, *j*-spanwise direction, *k*-streamwise direction)

Case 1 (without tip-gap)			
row	$i \times j \times k$	nodes	blocks
HPT-Inlet	25×41×17	17,425	1
HPT-Stator	17×41×145	101,065	1
HPT-Rotor-Up	9×41×69	25,461	1
HPT-Rotor-Inlet	17×41×9	6,273	1
HPT-Rotor	17×41×133	92,701	1
HPT-Rotor-Outlet	17×41×9	6,273	1
HPT-Rotor-Down	9×41×57	21,033	1
LPT-Rotor-Up	9×41×73	26,937	1
LPT-Rotor-Inlet	17×41×9	6,273	1
LPT-Rotor	17×41×97	67,609	1
LPT-Rotor-Outlet	17×41×33	23,001	1
LPT-Rotor-Down	9×41×73	26,937	1
Case 2 (with tip-gap)			
row	$i \times j \times k$	nodes	blocks
HPT-Inlet	25×41×17	17,425	1
HPT-Stator	17×41×145	101,065	1
HPT-Rotor-Up	9×57×49	25,137	1
HPT-Rotor-Inlet	17×57×9	8,721	1
HPT-Rotor	17×57×113	109,497	1
HPT-Rotor-Outlet	17×57×9	8,721	1

HPT-Rotor-Down	9×57×57	29,241	1
HPT-Rotor-Gap1	13×17×113	24,973	1
HPT-Rotor-Gap2	17×17×41	11,849	1
LPT-Rotor-Up	9×57×69	35,397	1
LPT-Rotor-Inlet	17×57×5	4,845	1
LPT-Rotor	17×57×97	93,993	1
LPT-Rotor-Outlet	17×57×33	31,977	1
LPT-Rotor-Down	9×57×69	35,397	1
LPT-Rotor-Gap1	13×17×97	21,437	1
LPT-Rotor-Gap2	17×17×33	9,537	1

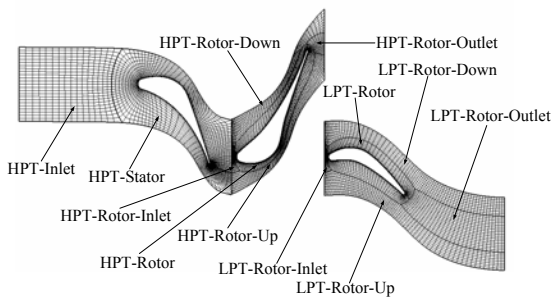

S1 Section (Midspan, Case 1 & Case 2)

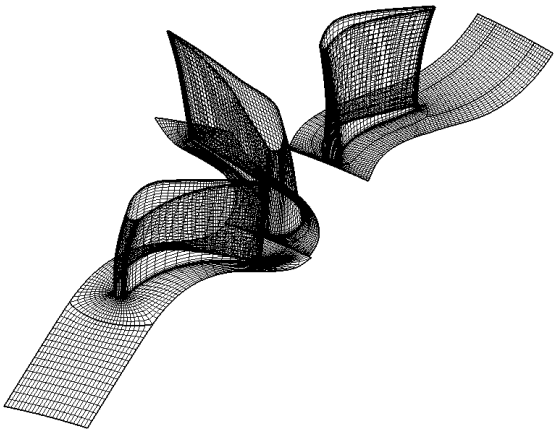

3D grid (Case 1 & Case 2)

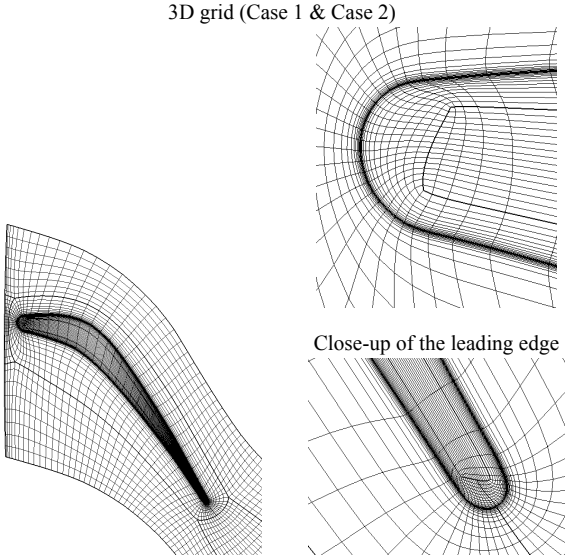

Close-up of the leading edge

Panorama

Close-up of the trailing edge

Grid of the LPR tip-gap (Case 2)

Fig. 2: H-O-H grid topologies of the VCRT

Validating of numerical code

In order to validate the predicted accuracy of the numerical code, a three-dimensional multistage unsteady Navier-Stokes simulation with inlet radial hot streak has been performed in a test turbine. Then the time-averaged numerical data are compared with the available experimental data. The test turbine is a 0.767 scale rig modeling the first stage of a two-stage core turbine designed for a modern high bypass ratio engine. The vane has a constant section, and was designed for a constant exit flow angle of 75° from axial. The rotor inlet was designed to accept the vane exit flow with either zero or slight negative incidence. The rotor outlet is a free-vortex design. Both vane and blade axial chords are constant radially. The experimental turbine has 26 vane airfoils and 48 rotor airfoils. It was tested in the NASA Lewis Research Center's WCTTR (Stabe et al. 1984, [22]; Dorney et al. 1999, [35]). The test conditions for the turbine are shown in Table 3.

Table 3: Flow conditions in the NASA test turbine

Inlet total temperature (K)	672.2
Inlet total pressure (Pa)	3.103×10^5
Mass flow (kg/s)	6.13
Specific work (J/kg)	1.299×10^5
Rotational speed (RPM)	11373
Total pressure ratio	2.36
Load factor	1.675
Flow coefficient	0.449

The inlet radial temperature profile in the experiment was produced using the CERTS (Combustor Exit Radial Temperature Simulator) inlet which injected cool air through circumferential slots in the hub and tip end walls upstream of the vane. Figure 3 shows the inlet radial temperature distribution. The ratio of the maximum total temperature to the average total temperature is approximately 1.05, and the ratio of maximum to minimum total temperature is approximately 1.20 at the turbine inlet.

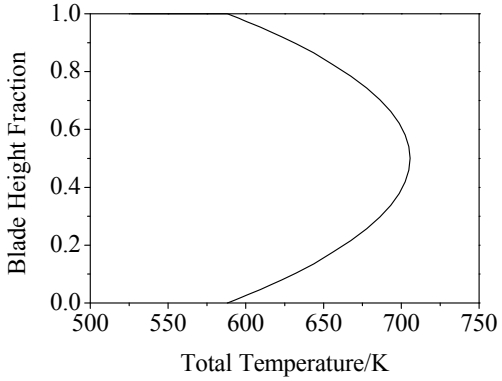

Fig. 3: Turbine inlet radial temperature profile

For reducing the cost of the calculation, the number of vanes in the first row is decreased to 24 and the size

of the vane is increased by a factor of 26/24 to maintain the same blockage. So, a 1-vane/2-rotor airfoil count ratio is used in the unsteady numerical simulation.

Figures 4 to 6 show comparisons between the predicted and experimental time-averaged critical velocity ratio distributions at the hub, midspan and tip of the vane. The predicted data are very close to the experimental data, except for near the trailing edge (TE) region of the vane and the suction surface at the tip of the vane.

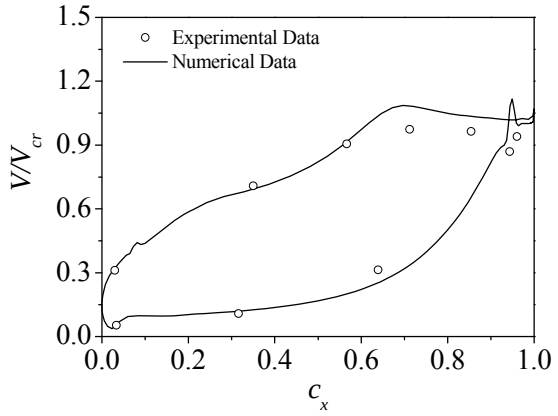

Fig. 4: Critical velocity ratio at the hub of the vane

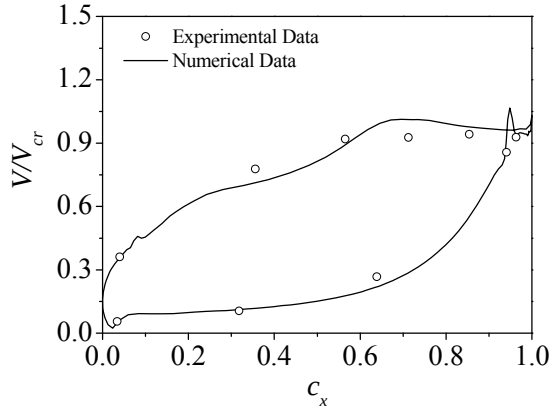

Fig. 5: Critical velocity ratio at the midspan of the vane

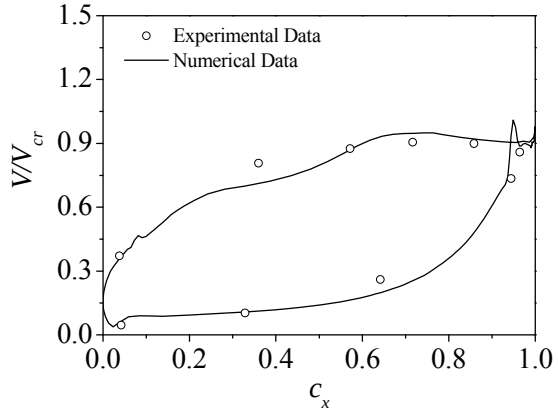

Fig. 6: Critical velocity ratio at the tip of the vane

Figure 7 illustrates the predicted and experimental total pressure distributions at the outlet of the turbine. There is a good agreement between the predicted and experimental results.

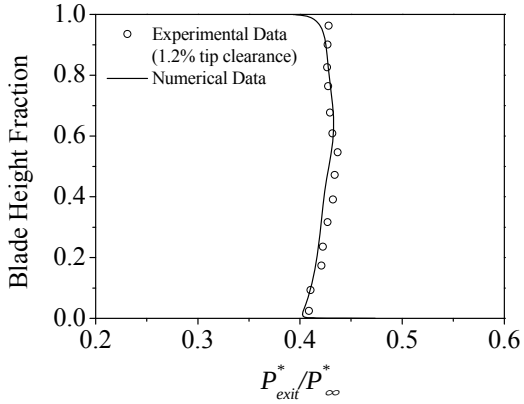

Fig. 7: Total pressure distribution at the outlet of the turbine

Figure 8 shows the predicted and experimental total temperature distributions at the outlet of the turbine. The predicted values show close agreement with the experimental values from hub to 70% span. The discrepancies near the tip region are due to the differences in the experimental (1.2%) and numerical (0%) tip clearances.

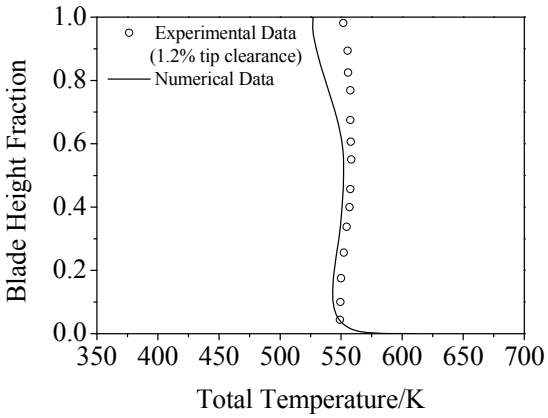

Fig. 8: Total temperature distribution at the outlet of the turbine

The above-mentioned results indicate that the predicted accuracy of the numerical code is acceptable in this investigation.

Inlet hot streak profile

In this paper, a hot streak temperature ratio of 2.0 is selected. The hot streak is circular in shape with a diameter equal to 25% of the HPT stator span. The hot streak center is located at 50% of the span and the leading edge of the HPT stator. The hot streak profile is shown in Fig. 9.

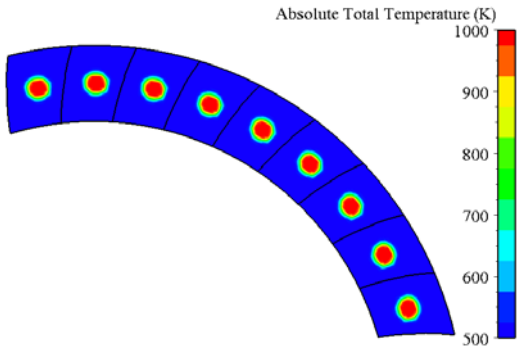

Fig. 9: Inlet hot streak profile (Case 1 & Case 2)

Numerical results

Figure 10 shows the static temperature contour on the midspan of the HPT rotor and LPR at one instant in time for case 1. The secondary flow and buoyancy cause the temperature redistribution in the HPT rotor when the hot streak mixes with the HPT vane wake and flows into the HPT rotor. Most of the hotter fluid convects towards the pressure surface of the HPT rotor, while most of the colder fluid migrates to the suction surface of the HPT rotor. And a few of hotter fluid also rounds the leading edge of the HPT rotor and migrates to the suction surface of the rotor. The hotter fluid, which has migrated to the pressure surface of the HPT rotor, goes through the HPT rotor along the pressure surface. It penetrates through the inner-extending shock wave (IESW) at the trailing edge of the HPT rotor and encounters the outer-extending shock wave (OESW) at the interface between the HPT rotor and the LPR. Then it mixes with the wake of the HPT rotor. And the OESW also has an effect on the mixed fluid. Finally, the mixed fluid is cut by the LPR and convects towards the pressure surface of the LPR. On the other hand, most of the colder fluid which has migrated to the suction surface of the HPT rotor goes through the HPT rotor along the suction surface. It penetrates through the IESW at about 60% axial chord of the HPT rotor and pierces the OESW at the trailing edge of the HPT rotor. After making an interaction with the OESW, it is cut by the LPR and migrates to the suction surface of the LPR. Due to a weak effect of leakage flow on the midspan fluid of the HPT rotor and the LPR, the temperature distribution on the midspan section in case 2 is very similar to the case 1.

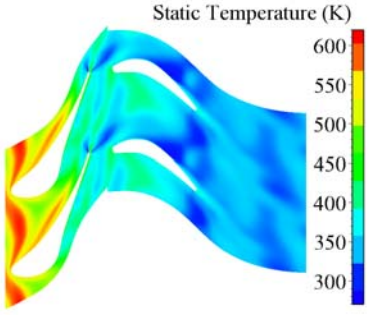

Fig. 10: Instantaneous static temperature contour on the midspan section of the HPT rotor and LPR-Case 1

Figure 11 describes the leakage flow in the LPR blade tip clearance. The fluid near the pressure surface tip region can be driven to the rotor suction surface by the leakage flow. In the LPR, some hotter fluid migrated to the pressure surface tip region will convect into the rotor the suction side. The migration induced by the leakage flow directly results in intensified heat load on the rotor suction surface. Figure 12 more clearly illustrates the above mentioned phenomenon. Figure 12 also shows that the gas temperature near to the casing wall is higher than the hot streak center temperature in the LPR. The tip high-temperature region is directly related to the leakage flow in the HPT rotor. In the HPT rotor, some high-temperature gas migrated into the tip clearance will go through the HPT rotor along the gap and convect into the LPR. The migration of the high-temperature gas induces the extreme high-temperature region at the tip region of the LPR.

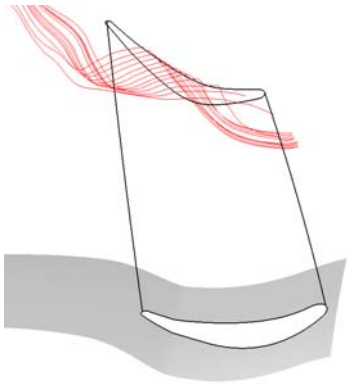

Fig. 11: LPR blade tip leakage flow

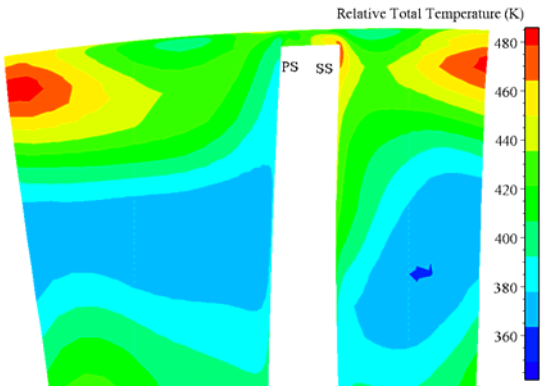

Fig. 12: Instantaneous temperature contour on a cross section (S3 section) of the LPR passage-Case 2

Figures 13 and 14 show the instantaneous temperature distribution at the LPR inlet for case 1 and case 2, respectively. Compared the results in Figs. 13 and 14, it is well know that the leakage flow in the HPT rotor trends to increase the LPR inlet temperature at the tip region. The phenomenon is coherent with the Fig. 12. The air flow with higher temperature at the tip region of the LPR inlet will affect the flow and heat transfer characteristics in the downstream LPT.

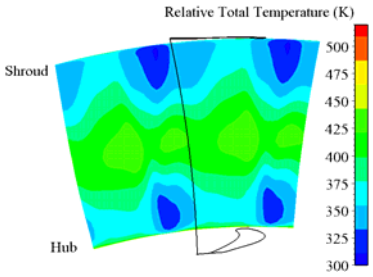

Fig. 13: Instantaneous temperature contour at the LPR inlet-Case 1

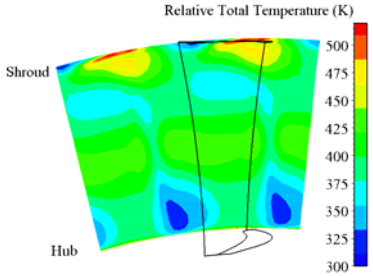

Fig. 14: Instantaneous temperature contour at the LPR inlet-Case 2

Figure 15 shows the time-averaged static temperature contour on the LPR for the case 1 (without tip clearance). There are two regions elevated adiabatic wall temperature on the suction surface. The larger high-temperature region originates from the hub at about 15% axial chord, and extends radially towards the trailing edge. The second high-temperature region emanates from the tip at the leading edge, and extends inverse-radially to the 50% axial chord at about 88% span. These two high-temperature regions are directly associated with the secondary flow in the LPR. The result has been proved in ref. [36]. In addition to the influence of secondary flow, the shock wave in the LPR also makes an effect on the high-temperature region, which emanates from the hub. So, the high-temperature region originating from the hub is directly related to the interaction between the secondary flow and the shock wave. Figure 15 indicates that there is still a larger high-temperature region on the suction surface of the LPR besides the above-mentioned two high-temperature regions. The high-temperature region is directly induced by the inlet hot streak. The region emanates from the leading edge, and extends axially towards the trailing edge. The radial extent of this region decreases approaching the trailing edge due to the effect of the secondary flow. Figure 15 also shows that there is a larger high-temperature region on the pressure surface of the LPR, which is associated with the inlet hot steak. The region originates from the leading edge, and extends axially towards the trailing edge. The radial extent of this region increases approaching the trailing edge due to the influence of the secondary flow. The temperature distribution on the LPR surface indicates that most of hot streak fluid migrates towards the pressure surface as it convects into the LPR. The migrating characteristics of the hot streak fluid are dominated by the secondary flow in the LPR. The effect of the buoyancy on the high-temperature fluid near the LPR blade surface is very weak. On the pressure surface of the LPR, the secondary flow drives the hotter fluid towards the hub and tip. While on the suction surface of the LPR, the secondary flow makes the hotter fluid migrate towards the midspan.

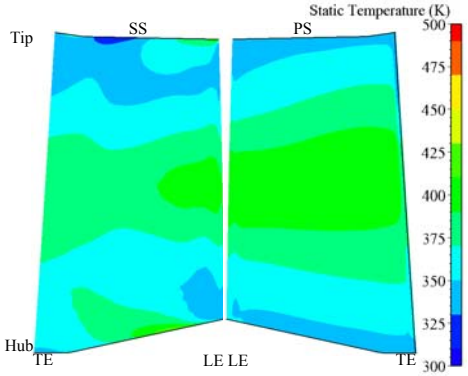

Fig. 15: Time-averaged static temperature contour on the LPR (Case 1)

Figure 16 shows the time-averaged static temperature contour on the LPR for the case 2 (with tip clearance). There are three regions elevated adiabatic wall temperature on the suction surface of the LPR. The first high-temperature region related to the interaction between the secondary flow and the shock wave originates from the hub at about 15% axial chord, and extends radially to the trailing edge at about 25% span. The second high-temperature region associated with the combined effects of secondary flow and tip leakage flow emanates from the tip at the leading edge, and extends inverse-radially to the trailing edge at about 65% span. The third high-temperature region related to the inlet hot streak emanates from the leading edge, and extends axially towards the trailing edge. The radial extent of this region decreases approaching the trailing edge due to the effect of the secondary flow. On the suction surface of the LPR, the secondary flow drives the hot streak fluid towards the midspan. On the other hand, the tip leakage flow also takes an effect on the hot streak fluid migrated to the suction surface of the LPR. The tip leakage flow induces the hot streak fluid migrate towards the hub on the suction surface of the LPR. It is well know that the temperature of the second high-temperature region is highest compared with the other two high-temperature regions. The reason is that the leakage flow in the HPT rotor directly drives hotter fluid towards the tip region of the LPR. Then the secondary flow and leakage flow will drive the hotter fluid to the trailing edge of the LPR along the inverse-radial and axial direction. The migration of the hotter gas induces the extreme high-temperature region at the tip region of the LPR. Figure 16 also shows that there is a larger high-temperature region on the pressure surface of the LPR, which is related to the inlet hot steak. The region originates from the leading edge, and extends axially towards the trailing edge. The radial extent of this region increases approaching the trailing edge due to the influence of the secondary flow and tip leakage flow. On the

pressure surface of the LPR, the secondary flow drives the hotter fluid towards the hub and tip, and the leakage flow drives the hotter fluid towards the tip. The migration of the hotter fluid on the pressure surface directly induces the high-temperature region. The temperature distribution on the LPR surface also indicates that most of hot streak fluid migrates towards the pressure surface as it convects into the LPR. The migrating characteristics of the hot streak fluid are dominated by the combined effects of the secondary flow and tip leakage flow in the LPR.

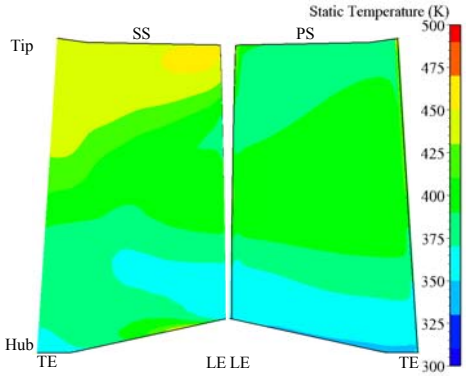

Fig. 16: Time-averaged static temperature contour on the LPR (Case 2)

It is well know that the heat load of the LPR is intensified due to the effects of the tip leakage flow through the comparison between fig. 15 and fig.16.

Figure 17 indicates the time-averaged relative total temperature distributions in the LPR passages for case 1 and case 2. In these two cases, the secondary flow drives the hot streak fluid towards the pressure surface along the flow direction. When the hot streak fluid migrates to the pressure surface, the secondary flow will drive it towards the hub and tip along the flow direction. And the secondary flow also drives the colder fluid towards the suction surface along the flow direction companying the hot steak fluid movements. As the colder fluid migrates to the suction surface, the secondary flow drives the colder fluid towards the midspan along the flow direction. A little of hot streak fluid, which rounds the leading edge of the LPR and migrates to the suction surface, also moves towards the midspan along the flow direction under the effect of the secondary flow. Compared the results between case 1 and case 2 in Fig. 17, it is well known that the radial migration of the hot streak fluid is also dominated by the leakage flow in the rotor tip clearance. The leakage flow trends to drive the hotter fluid towards the blade tip on the pressure surface and to the hub on the suction surface. Figure 17 also indicates that the hotter fluid migrated to the tip region at the leading edge of the LPR through the tip clearance of the HPT rotor moves across the tip-gap of the LPR and reaches the suction surface. Then the secondary flow and leakage flow will drive the hotter fluid to the trailing edge of the LPR along the inverse-radial and axial direction. The migration of the hotter gas directly induces the extreme high-temperature region at the tip region of the LPR. Figure 18 more clearly shows the effects of the tip leakage flow on the hotter fluid. Figure 17 also shows that the leakage flow effect trends to increase the LPR outlet temperature at the tip region. In a word, the existence of the tip leakage flow directly results in a different temperature distribution in LPR between case 1 and case 2.

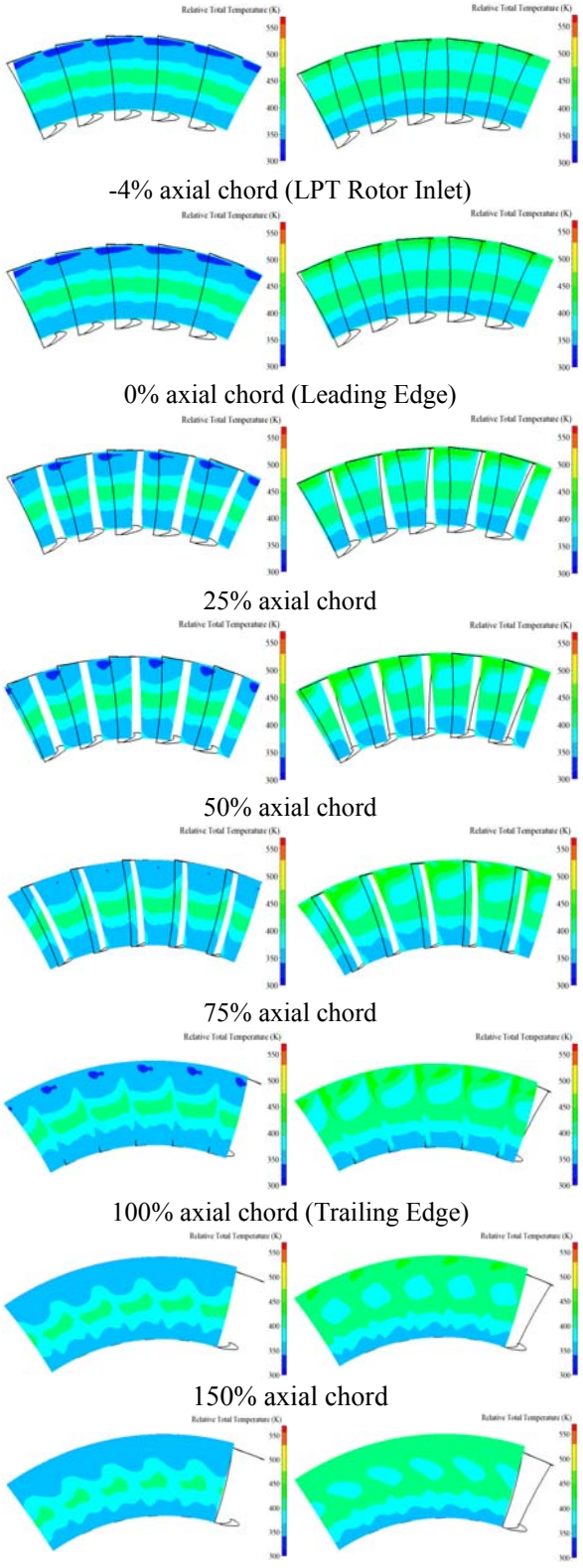

Fig. 17: Time-averaged relative total temperature contours on some S3 sections of the LPR passage

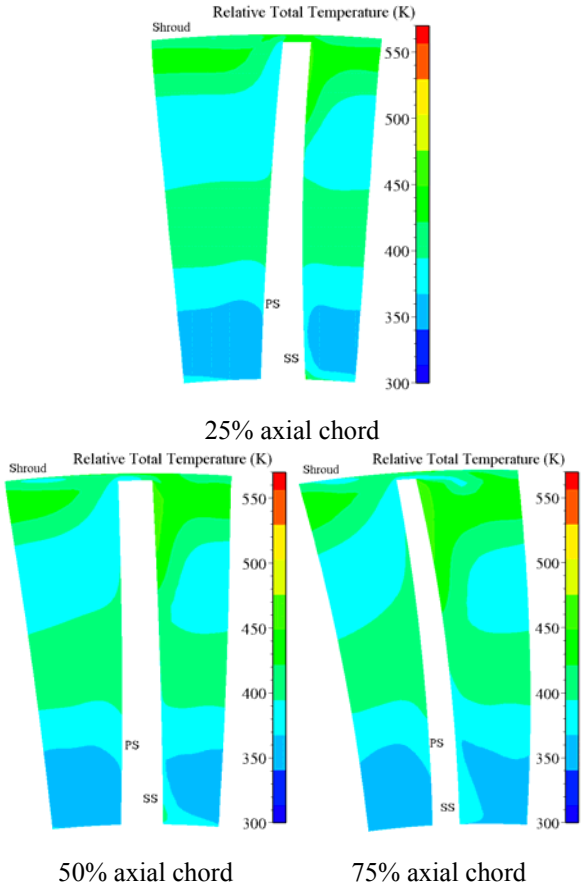

Fig. 18: Time-averaged relative total temperature contours on three S3 sections of the LPR passage-Case 2

Conclusions

This paper is to study the effects of the rotor tip clearance on the inlet hot streak migration characteristics in LPR of a VCRT. The major conclusions can be summarized as follows:

1) The hot streak is not mixed out by the time it reaches the exit of HPT rotor. The separation of colder and hotter fluid is observed at the LPR inlet. Most of hotter fluid migrates towards the rotor pressure surface, and only little hotter fluid migrates to the rotor suction surface when it convects into the LPR.

2) The hotter fluid migrated to the tip region of the HPT rotor impinges on the leading edge of the LPR after it goes through the HPT rotor. The secondary flow and leakage flow will drive the hotter fluid to the trailing edge of the LPR along the inverse-radial and axial direction. The migration of the hotter fluid directly induces an extreme high-temperature region at the tip region of the LPR.

3) The migration characteristics of the hot streak in the LPR are dominated by the combined effects of secondary flow and leakage flow at the tip clearance.

4) The leakage flow trends to drive the hotter fluid towards the blade tip on the pressure surface and to the hub on the suction surface.

5) The leakage flow trends to increase the heat load of the LPR blade and the temperature at the tip region of the LPR outlet.

References

[1] B.D. Keith, D.K. Basu and C. Stevens. Aerodynamic test results of Controlled Pressure Ratio Engine (COPE) dual spool air turbine rotating rig. ASME Paper 2000-GT-0632, 2000.

[2] C.W. Haldeman, M.G. Dunn, R.S. Abhari, P.D. Johnson and X.A. Montesdeoca. Experimental and computational investigation of the time-averaged and time-resolved pressure loading on a vaneless counter-rotating turbine. ASME Paper 2000-GT-0445, 2000.

[3] Q.J. Zhao, H.S. Wang, X.L. Zhao and J.Z. Xu. Numerical analysis of 3-D unsteady flow in a vaneless counter-rotating turbine. *Journal of Engineering Thermophysics*, Vol. 27, No. 1, 2006, pp. 35-38.

[4] Q.J. Zhao, H.S. Wang, X.L. Zhao and J.Z. Xu. Three-dimensional numerical investigation of vaneless counter-rotating turbine. *Journal of Propulsion Technology*, Vol.27, No. 2, 2006, pp. 114-118.

[5] W.T. Wintucky and W.L. Stewart. Analysis of two-stage counter-rotating turbine efficiencies in terms of work and speed requirements. NACA RM E57L05, 1958.

[6] J.F. Louis. Axial flow contra-rotating turbines. ASME Paper 85-GT-218, 1985.

[7] M. Munk and R.C. Prim. On the multiplicity of steady gas flows having the same streamline pattern. *Proceedings of the National Academy of Sciences, U.S.* Vol. 33, 1947, pp. 137-141.

[8] B. Lakshminarayana and J.H. Horlock. Generalized expressions for secondary vorticity using intrinsic coordinates. *Journal of Fluid Mechanics*, Vol. 59, 1973, pp. 97-115.

[9] T.L. Butler, O.P. Sharma, H.D. Joslyn and R.P. Dring. Redistribution of an inlet temperature distortion in an axial flow turbine stage. *AIAA Journal of Propulsion and Power*, Vol. 5, No. 1, 1989, pp. 64-71.

[10] M.M. Rai and R.P. Dring. Navier-Stokes analyses of the redistribution of inlet temperature distortions in a turbine. *AIAA Journal of Propulsion and Power*, Vol. 6, No. 3, 1990, pp. 276-282.

[11] R.J. Roback and R.P. Dring. Hot streaks and phantom cooling in a turbine rotor passage: Part 1-separate effects. ASME Paper 92-GT-75, 1992.

[12] D.J. Dorney, R.L. Davis, D.E. Edwards and N.K. Madavan. Unsteady analysis of hot streak migration in a turbine stage. *AIAA Journal of Propulsion and Power*, Vol. 8, No. 2, 1992, pp. 520-529.

[13] D.J. Dorney and R.L. Davis. Numerical simulation of turbine 'hot spot' alleviation using film cooling. *AIAA Journal of Propulsion and Power*, Vol. 9, No. 3, 1993, pp. 329-336.

[14] D.J. Dorney. Numerical investigation of hot streak temperature ratio scaling effects. AIAA Paper 96-0619, 1996.
[15] O.P. Sharma, G.F. Pichett and R.H. Ni. Assessment of unsteady flows in turbines. ASME Paper 90-GT-150, 1990.
[16] K.L. Gundy-Burlet and D.J. Dorney. Three-dimensional simulations of hot streak clocking in a 1-1/2 stage turbine. AIAA Paper 96-2791, 1996.
[17] T. Shang and A.H. Epstein. Analysis of hot streak effects on turbine rotor heat load. *ASME Journal of Turbomachinery*, Vol. 119, No. 3, 1997, pp. 544-553.
[18] R.P. Dring, M.F. Blair, H.D. Joslyn, G.D. Power and J.M. Verdon. The effects of inlet turbulence and rotor/stator interactions on the aerodynamics and heat transfer of a Large-Scale Rotating Turbine Model. NASA-CR-4079, 1987.
[19] O.P. Sharma, G.M. Stetson, W.A. Daniels, E. M. Greitzer, M.F. Blair and R.P. Dring. Impact of periodic unsteadiness on performance and heat load in axial flow turbomachines. NASA-CR-202319, 1997.
[20] W.J. Whitney, R.G. Stabe and T.P. Moffitt. Description of the warm core turbine facility recently installed at NASA Lewis Research Center. NASA-TM-81562, 1980.
[21] J.R. Schwab, R.G. Stabe and W.J. Whitney. Analytical and experimental study of flow through an axial turbine stage with a nonuniform inlet radial temperature profile. NASA-TM-83431, 1983.
[22] R.G. Stabe, W.J. Whitney and T.P. Moffitt. Performance of a high-work low-aspect ratio turbine tested with a realistic inlet radial temperature profile. AIAA Paper 84-1161, 1984.
[23] G.R. Guenette. A fully scaled short duration turbine experiment. Sc.D. Thesis, MIT, 1985.
[24] D.D. Sujudi. An experimental investigation of the effects of inlet circumferential temperature distortion on the aerodynamic performance of a single stage turbine. Master's Thesis, MIT, 1994.
[25] T. Shang. Influence of inlet temperature distortion on turbine heat transfer. Philosophy Doctor's Thesis, MIT, 1995.
[26] T. Shang, G.R. Guenette, A.H. Epstein and A.P. Saxer. The influence of inlet temperature distortion on rotor heat transfer in a transonic turbine. AIAA Paper 95-3042, 1995.
[27] S.P. Harasgama. Combustor exit temperature distortion effects on heat transfer and aerodynamics within a rotating turbine blade passage. ASME Paper 90-GT-174, 1990.
[28] K.L. Gundy-Burlet and D.J. Dorney. Influence of 3D hot streaks on turbine heat transfer. *International Journal of Turbo and Jet Engines*, Vol. 14, No.3, 1997, pp. 123-131.
[29] L. Castillon, E. Laroche and O. Sgarzi. Unsteady three-dimensional Navier-Stokes analysis of a hot streak transport through an axial high pressure turbine stage. ISABE Paper 2003-1063, 2003.
[30] Fine Turbo User Manual 6-2-9, NUMECA International, 2005.
[31] A. Jameson. Time dependent calculations using multigrid with applications to unsteady flows past airfoils and wings. AIAA Paper 91–1596, 1991.
[32] A. Arnone and R. Pacciani. Rotor-stator interaction analysis using the Navier-Stokes equations and a multigrid method. *ASME Journal of Turbomachinery*, Vol. 118, No. 3, 1996, pp. 679-689.
[33] M.M. Rai. Three-dimension Navier-Stokes simulations of turbine rotor-stator interaction, Part I-Methodology. *AIAA Journal of Propulsion and Power*, Vol. 5, No. 3, 1989, pp. 305-311.
[34] P. Spalart and S. Allmaras. A one-equation turbulence model for aerodynamic flows. AIAA Paper 92-0439, 1992.
[35] D.J. Dorney, D.L. Sondak and P.G.A. Cizmas. Effects of hot streak/airfoil ratio in a high-subsonic single-stage turbine. AIAA Paper 99-2384, 1999.
[36] Q.J. Zhao, F. Tang, H.S. Wang, J.Y. Du, X.L. Zhao and J.Z. Xu. Influence of hot streak temperature ratio on low pressure stage of a vaneless counter-rotating turbine. ASME Paper 2007-GT-27028, 2007.

Nomenclature

a	Velocity of sound
c	Nondimensional chord
P	Static pressure
SWR	Ratio of specific work of the high pressure turbine to that of the low pressure turbine
T	Static temperature
u, v, w	x, y, z components of velocity
V	Absolute velocity
ρ	Density

Superscripts

*	Total quantity

Subscripts

6	LPR exit quantity
cr	Critical value
hs	Hot streak quantity
x	Axial direction
∞	Free stream quantity